*Journal of Engineering Physics and Thermophysics, Vol. 74, No. 4, 2001*

# HEAT EXCHANGE IN THE CLASSICAL CZOCHRALSKI METHOD

**V. S. Berdnikov, V. V. Vinokurov, V. I. Panchenko, and S. V. Solov'ev**

UDC 532.529.2;536.24;621.746

*Numerically, by the method of finite differences, we investigated the regimes of laminar convection of a thermogravitational, thermocapillary, and gravitational-capillary nature in the classical variant of the Czochralski method. Evolution of the spatial form of flow in each type of convection and the trends of local and integral heat exchange in the range of Grashof, $0 \le Gr \le 8 \cdot 10^4$, and Marangoni, $0 \le Ma \le 6.5 \cdot 10^4$ numbers have studied for the Prandtl number Pr = 16. Local heat exchange in the regimes of free and mixed convection is investigated experimentally.*

Perfect bulk single crystals represent a starting material for micro- and optoelectronics nonlinear optics, and laser equipment. For industrial and research purposes. They are produced by different methods of drawing from a melt, in particular, by different variants of the Czochralski method [1–6]. Free and mixed convection near a cold disk located axisymmetrically on the free surface of the liquid that fills, up to the level $z = H$, a cylindrical vessel with uniformly heated side walls can form a simplified model of the processes of convective heat exchange in the Czochralski method. This system is the subject of experimental and numerical investigations in [1–5] and in the present work. The current interest in the study is explained by the fact that the quality of single crystals depends on the processes of transfer near the crystallization front that create specific thermodynamic conditions of liquid–solid body transition. These conditions are determined by the local temperature field, which depends on the hydrodynamics of a melt, radial and azimuthal distributions of local fluxes of heat and impurities, levels of the amplitudes of temperature fluctuations, their frequency ranges, and distributions of the scales of secondary flows [1, 5]. In actual technological practice and in our physical model, the hydrodynamics of the melt is determined by the mutual action of a complex of mass and surface forces. In this connection there is a problem of determining the relative contribution of each of the forces in the formation of flow structure of the melt and analysis of the results of their nonlinear interaction. A fruitful path in solving the problem is the carrying out of coordinated experimental and numerical investigations. For an isothermal forced flow these investigations were undertaken in [3] to justify the adequacy of the physicomathematical model and methods of numerical simulation [3, 4, 6].

In the present work, we carried out experimental investigations of local heat exchange in the regimes of thermal gravitational-capillary and mixed (during rotation of only the model of a crystal) convection from a laminar to a developed turbulent regime of flow. The general aim of the experiments [1–5] was to determine the boundary of transition to nonstationary three-dimensional flows and quantitative investigations of characteristics in transient and turbulent regimes. In a continuation of [3, 4], numerical simulation (by the method of finite differences) of thermal gravitational-capillary convection is performed, which was coordinated with a physical experiment [4, 5]. The aim of the numerical investigations was to simulate the evolution of flow in the regime of thermogravitational convection with increase in Gr, then of thermocapillary

S. S. Kutateladze Institute of Thermophysics, Siberian Branch of the Russian Academy of Sciences, Novosibirsk, Russia; email: berdnikov@itp.nsc.ru. Translated from Inzhenerno-Fizicheskii Zhurnal, Vol. 74, No. 2, pp. 122–127, July–August, 2001. Original article submitted September 11, 2000.

1062-0125/01/7404-1007$25.00 

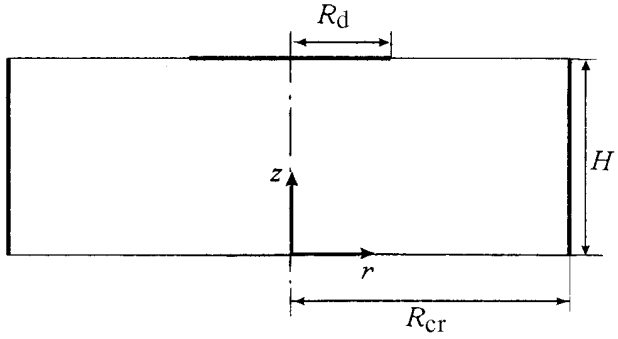


Fig. 1. Scheme of computational region

convection with increase in Ma, and, finally, of thermal gravitational-capillary convection and elucidation of the relative role of buoyancy forces and of the thermocapillary effect.

An idealized physicomathematical model of the processes considered is the thermal gravitational-capillary and mixed contion near different-diameter disks that partially close the free surface of the liquid that imitates a melt (Fig. 1). The container has a cylindrical symmetry and fixed rectilinear boundaries. The crystallization front is plane; it is located at the level of the free surface of the melt. In the numerical model for the velocity field on the boundary of the crucible and at the crystallization front the no-slip conditions are fulfilled. On the free surface of the melt, the condition of balance is set between the tangential component of the force, attributable to the surface tension gradient, and the forces of friction in the regime of thermocapillary convection and the absence of friction in the regime of thermogravitational convection. Constant temperatures of the crystal and of the side wall of the container are prescribed. The condition of thermal insulation is set on the bottom and free surface of the liquid. The initial system of dimensionless equations of free convection in the Boussinesq approximation, on the assumption of axial symmetry of the fields of motion and temperature, in the vortex, stream function, and temperature variables, and the conditions for all the elements of the boundary are formulated mathematically as [6]

$$\frac{\partial\omega}{\partial t}+U\frac{\partial\omega}{\partial r}+V\frac{\partial\omega}{\partial z}-\frac{U\omega}{r}=\left(\Delta\omega-\frac{\omega}{r^2}\right)-\mathrm{Gr}\frac{\partial\theta}{\partial r};\quad \Delta\psi-\frac{2}{r}\frac{\partial\psi}{\partial r}=r\omega;\quad \frac{\partial\theta}{\partial t}+U\frac{\partial\theta}{\partial r}+V\frac{\partial\theta}{\partial z}=\frac{1}{\mathrm{Pr}}\Delta\theta;$$

1) bottom of the crucible: $\psi = 0$, $\frac{\partial\psi}{\partial z} = 0$, $\frac{\partial\theta}{\partial z} = 0$, $z = 0$, $0 \le r \le 2.76$;

2) side surface: $\psi = 0$, $\frac{\partial\psi}{\partial r} = 0$, $\theta = 1$, $0 \le z \le H$, $r = 2.76$;

3) free surface: $\psi = 0$, $\omega = -\frac{\mathrm{Ma}}{\mathrm{Pr}}\frac{\partial\theta}{\partial z}$, $z = H$, $1 \le r \le 2.76$;

4) crystallization front: $\psi = 0$, $\frac{\partial\psi}{\partial z} = 0$, $\theta = 0$, $z = H$, $0 \le r \le 1$;

5) symmetry axis: $\psi = 0$, $\omega = 0$, $\frac{\partial\theta}{\partial r} = 0$, $0 \le z \le H$, $r = 0$.

The quantity $R_d$ is used as the length scale, $\Delta T$ as that of temperature; and $\nu/R_d$ that of velocity. Below we present the results of calculations for the liquid with Pr = 16 and for the fixed geometry selected earlier [1–6] for test experiments: $H/R_d = 0.7$; $R_{cr}/R_d = 2.76$. The system of equations is solved using an implicit difference scheme. In solving the equation, the method of separation of variables was used for the stream function with the aid of a fast Fourier transform. Central differences are used. The equations of heat and momentum transfer are approximated using a difference scheme of variable directions of Pismen–Reck-

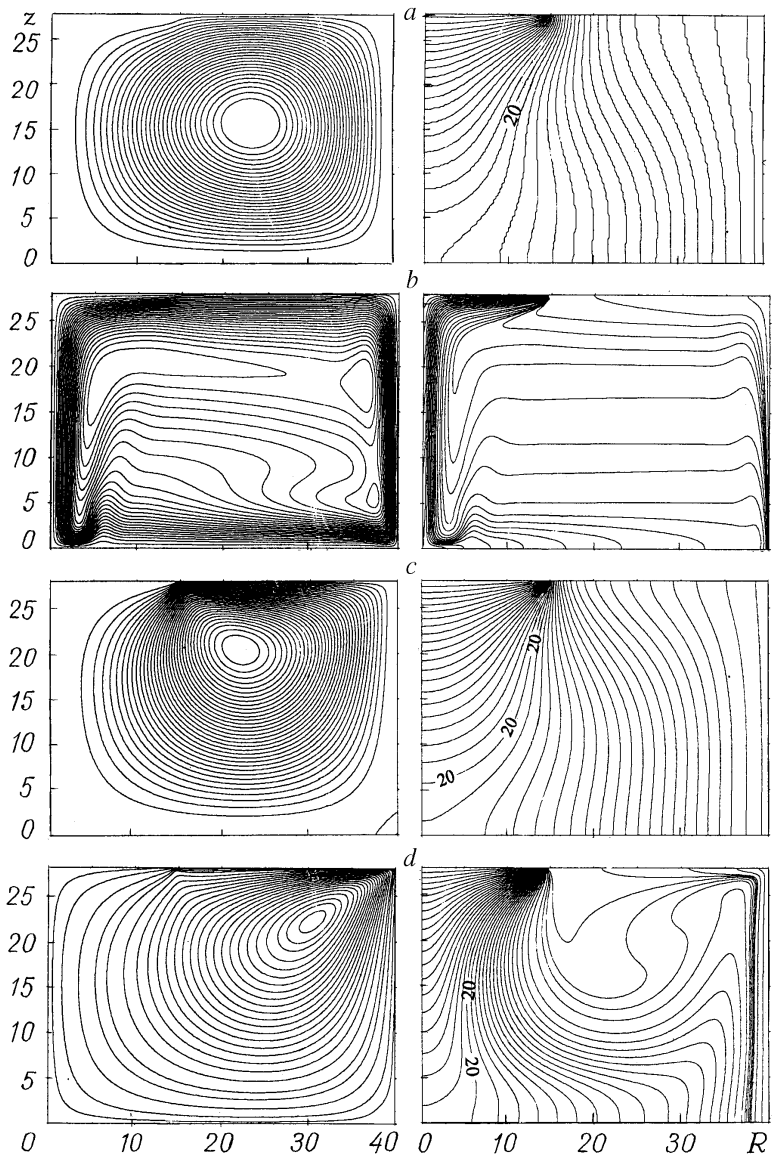


Fig. 2. Isolines of the stream function and isotherms in the regimes of thermogravitational convection [Ma = 0; a) Gr = 10; b) 78,275] and thermocapillary convection [Gr = 0; c) Ma = 100; d) 23,756]. *z*, *R*, mm.

ford [7]. At each half-step the convective terms of the equation are taken from the previous half-step. The equations are reduced to systems with a three-diagonal matrix and are solved by the pivot method.

The evolution of the thermal gravitational convection structure with increase in the Gr number without account for the thermocapillary effect is shown in Fig. 2a,b, and the evolution of the thermocapillary flow with increase in Ma is demonstrated in Fig. 2c, d. Figure 3 shows the development of thermal gravitational capillary convection with increase in Gr for constant Ma. Figures 2 and 3 show only the right side of an axisymmetric flow. The differences of the spatial forms of flow of thermocapillary and thermogravitational nature [2] are reduced to the following. In the regime of thermal gravitational convection, a descending cold jet on the axis from below the cooled disk and an ascending semijet on the hot walls of the container make identically a great contribution to the formation of the flow circulatory over the contour, i.e., a meridian flow. In this regime the liquid is actively drawn under the cold surface of the crystallization front. By its physical nature, the thermocapillary flow has a near-surface character, the active force acts only along the free surface,

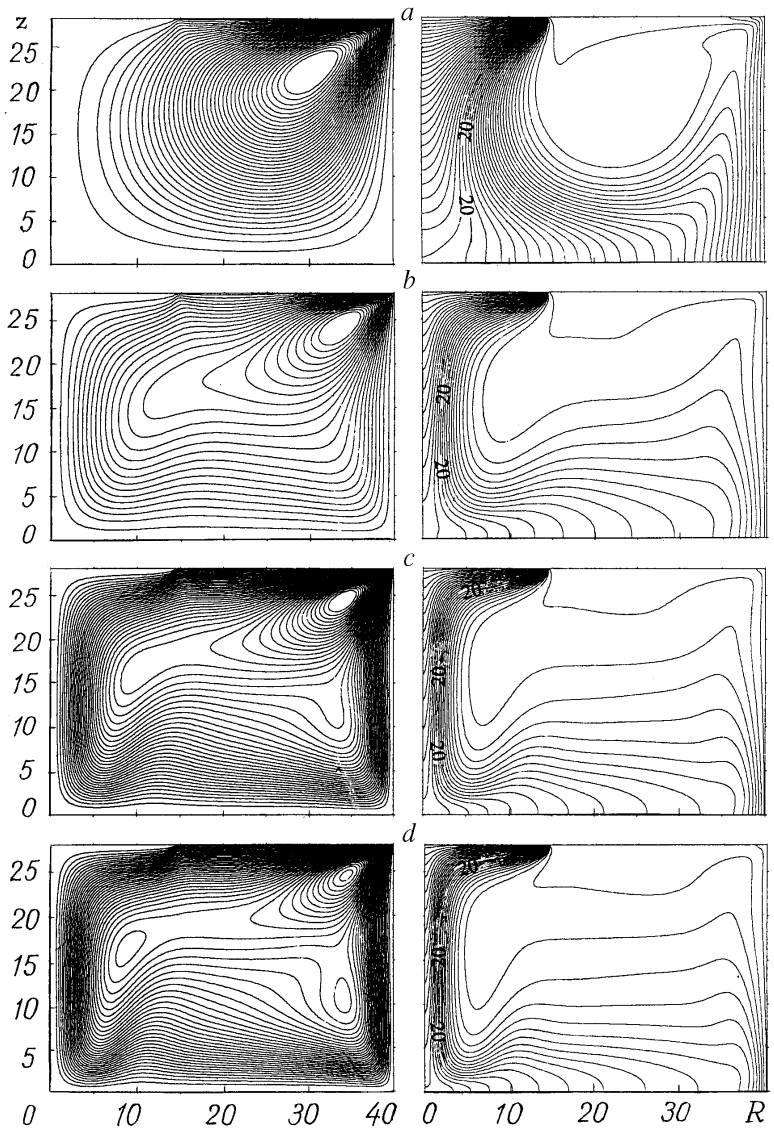


Fig. 3. Evolution of the structure of flow in the regime of thermal gravitational-capillary convection with increase in the Gr number [Ma = 34,240; a) Gr = 0; b) 1000; c) 3000; d) 10,000].

and the hot liquid from the wall of the vessel occurs under the cold surface only by inertia. The liquid is elongated along the wall of the vessel from the depth due to the continuity effect. Nevertheless, it is seen that the deep liquid layers are entrained also into this type of convection even at relatively small values of Ma (Fig. 2c). The position of the center around which the meridian circulation of the liquid occurs also differs greatly. As Ma increases, in the thermal capillary convection this center shifts into the corner between the wall of the crucible and the free surface. In the regime of thermal gravitational convection, as Gr increases, there is a distinct tendency toward the formation of two centers located approximately at the level of half the height of the liquid and displaced to the ascending and descending flows.

The differences in the hydrodynamics [2–4] exert their influence also on the distribution of temperature in the bulk of the liquid. In the regime of thermocapillary convection, as Ma increases, a kind of "thermal bag" is formed under the free surface (Figs. 2d and 3a) from which heat flows under the cold disk and into the tongue of the cold liquid drawn from the bottom along the wall of the container, i.e., with increase

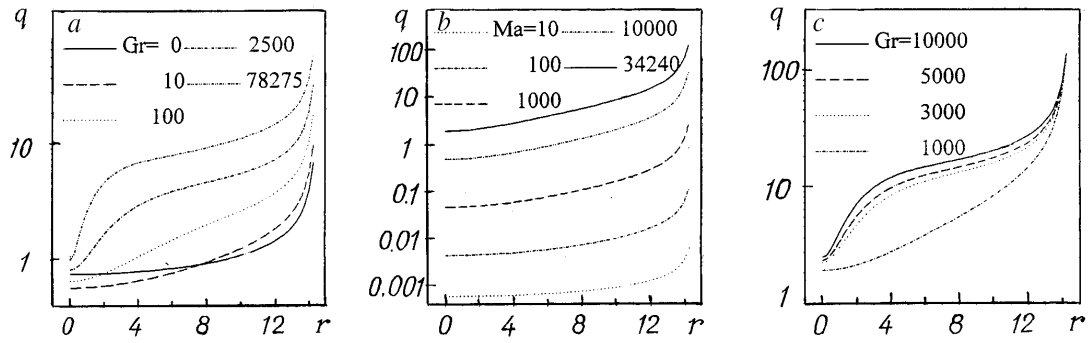


Fig. 4. Radial distribution of local heat fluxes on the model front of crystallization in the regimes of thermogravitational convection (a); thermocapillary convection (b), and thermal gravitational-capillary convection (c); Ma = 34,240. $q$, W/m$^2$; $r$, mm.

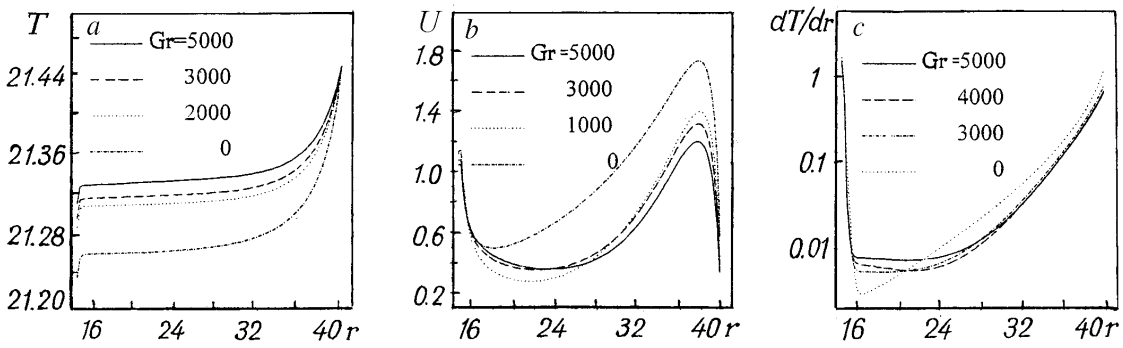


Fig. 5. Radial distributions on the free source of: a) temperature; b) radial component of velocity; c) dimensionless local gradient of temperature. $T$, $^{o}$C; $U$, mm/sec.

in Ma the structure of the temperature field differs increasingly from that observed in the regime of thermogravitational convection. As a result, even with qualitatively identical fields of isotherms (Fig. 2a, c), radial distributions of the local heat flux on the disk differ sharply qualitatively and quantitatively (Fig. 4a, b): in the regime of thermocapillary convection a splash on the edge is observed, but in the region of $0 \le r \le R_d/2$ the heat flux is negligible. In the regime of thermogravitational convection, the local heat flux also has a maximum on the edge, but heat transfer is substantial over the entire surface of the disk except for the axial region (Fig. 4a).

In numerical investigations of the simultaneous thermal gravitational-capillary convection, first thermocapillary convection was investigated at Ma = 34,240, which corresponds to the experimentally realizable regime of thermal gravitational capillary convection. Then an increasingly more intense gravity field is applied, the Gr number is correspondingly is increased, i.e., the evolution of the flow structure (Figs. 3 and 5) with increase in the relative contribution of buoyancy forces at a fixed Ma is investigated. With application of even a weak gravity field a cold descending jet appears from below the cold surface. The meridian circulation of liquid over the contour of the liquid begins, which has a thermogravitational nature (Fig. 3b). With increase in Gr, the spatial organization of flow more and more corresponds in detail to that observed experimentally [1]: this is circulation around the external contour and the meridian vortex (built into the main one), which is located near the surface and has a thermocapillary nature. As the number Gr increases, the absolute values of the velocity also approach the experimentally measured ones [1, 5]. Figure 5 presents the local characteristics of velocity and temperature fields that allow one quantitatively and qualitatively to evaluate their rearrangement with increase in the influence of buoyancy forces. A tendency toward a change to the

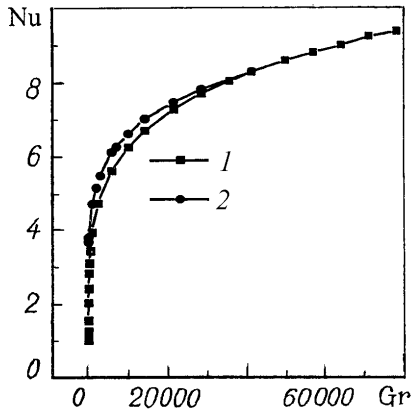


Fig. 6. Dependence of the dimensionless integral coefficient of heat transfer on the number Gr in the following regimes: 1) thermogravitational convection [Ma = 0; Nu = $(0.937 \pm 0.019)\mathrm{Gr}^{0.2051\pm0.0021}$]; 2) thermal gravitational-capillary convection (Ma = 34,240).

form typical of the regime of thermogravitational convection is characteristic of the distributions of velocity (Fig. 5b), temperature (Fig. 5a), and temperature gradient (Fig. 5c) along the free surface with increase in Gr, but it is seen that here the influence of the thermocapillary effect (up to Gr = 5000 at Ma = 34,240) is simply dominating. The increasing effect of thermogravitational convection exerts a noticeable influence on the radial distribution of the heat flux on the disk in the region $0 \le r \le R_d/2$ (Fig. 4c). We may say that it is entirely attributable to the thermogravitational convection in this region.

Figure 6 shows the dependence of the dimensionless heat-transfer coefficient, i.e., of the Nusselt number Nu, on Gr for Ma = 34,200. When Gr = 0, Nu = 3.80 and it is entirely determined by thermocapillary convection. As Gr increases, the values of Nu tend asymptotically to the values determined by thermogravitational convection: in the regime of thermogravitational convection, when Gr = 21,000 and Ma = 34,240, Nu = 8.82, whereas in the regime of thermogravitational convection at the same value of Gr, Nu = 8.29. Comparison of the distributions of $q(r)$ in Fig. 4 allows the following conclusions to be made: (1) the drawing of single crystals in weightlessness from a free surface in the regime of thermocapillary convection is less technological than in the gravity field; (2) the regime of thermal gravitational-capillary convection is also not optimal on account of a strong radial nonuniformity in the distributions of $T(r)$ and $q(r)$. These data clearly show why technologists must apply rotation of a crystal and seek, by the trial and error method, the optimum angular speed of its rotation which depends on Gr and Ma. The experimental data on radial distributions of $q$ in the regimes of thermal gravitational-capillary convection and mixed convection obtained on the experimental rig described in detail in [5] are presented in Fig. 7. Here, the open symbols denote the results of measurements by a two-junction probe (differential thermocouple) and the filled symbols denote the results of measurements by a single-junction probe. In the latter case, the local heat flux is determined by the mean temperature profile. The results presented in Fig. 7a were obtained for $R_{cr}/R_d$ = 1.6; $H/R_{cr}$ = 1.25; Re = 0; Gr = $2.4\cdot10^7$ (1, 2); Re = $5\cdot10^3$; Gr = $2.7\cdot10^7$ (3, 4); Re = $1.5\cdot10^4$; Gr = $2.1\cdot10^7$ (5, 6); Re = $3\cdot10^4$; Gr = $1.5\cdot10^7$ (7, 8); and in Fig. 7b for: $R_{cr}/R_d$ = 1.6; $H/R_{cr}$ = 0.75; Re = 0; Gr = $2.3\cdot10^7$ (1, 2); Re = $5\cdot10^3$; Gr = $2.7\cdot10^7$ (3, 4); Re = $1.4\cdot10^4$; Gr = $2.9\cdot10^7$ (5, 6); Re = $3\cdot10^4$; Gr = $1.45\cdot10^7$ (7, 8). These results were obtained on a working section with $D_{[c}r\}$ = 295 mm. Qualitatively, they are typical of both other $R_{cr}/R_d$ and of the case $D_{cr}$ = 80 mm [2, 4, 5]. The difference from the above-given results of numerical simulation consists of the fact that in the boundary layers on the cold disk in the regime of thermal gravitational-capillary convection there occurs a laminar-turbulent transition (curves 1 in Fig. 7). The flow is nonstationary and substantially three-dimensional [5]. The switching-on of the rotation of the disk leads to the formation of a centrifugal vortex (at the threshold value of Re), in which the direction

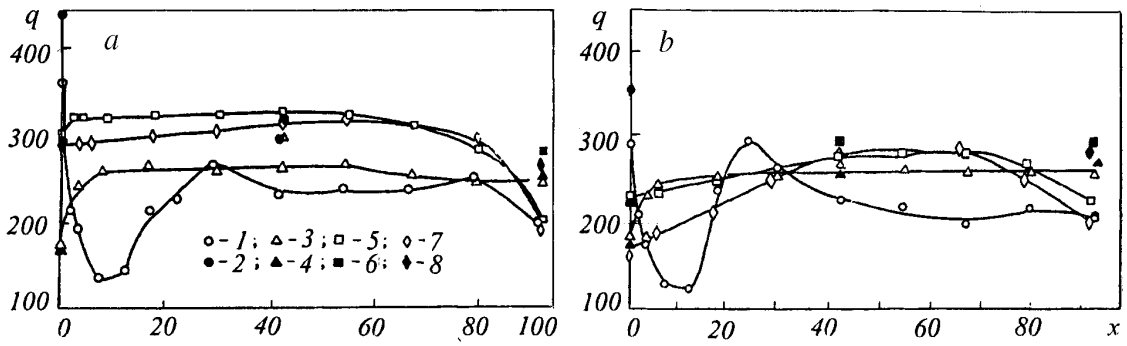


Fig. 7. Dependence of radial distributions of local heat fluxes on the angular velocity of rotation of the crystal model. $q$, W/m$^2$; $x$, mm.

of flow is opposite to the flow in thermal gravitational-capillary convection: the ascending flow on the axis, thereafter the liquid moves to the periphery of the disk, collides with the free-convective flow, and goes downward into the liquid core. After this, the liquid moves closer to the symmetry axis and is entrained by the ascending flow. The spatial form of flow in the meridian section represents an internal torus of a centrifugal nature, and an external torus of irregular shape, i.e., a large-scale centrifugal vortex is formed under the disk and a free-convective one beyond it. They have a common descending flow [1]. From the time of inception of the centrifugal vortex, its radial size is equal to the disk radius. Its radial size virtually does not change with increase in the Reynolds number, but its vertical size increases. The level of penetration of the vortex downwards, toward the bottom, and the volume of the liquid entrained into the forced flow depend on the relationship between Gr and Re [1]. At the threshold value of the Reynolds number that depends on Gr, the centrifugal vortex reaches the bottom. Thereafter, as the Reynolds number increases, its radial size grows, and the size of the outer free-convective torus-like vortex decreases accordingly. It is clear that in addition to the meridian motion the liquid has an azimuthal velocity component. The trajectories of liquid motion are windings on the inner and outer tori of irregular shape. The rearrangement of the hydrodynamics under the rotating disk is accompanied by the equilibration of $q(r)$. The most uniform distribution reflects the state in the range of values of Gr and Re between their values corresponding to curves 3 and 7 in Fig. 7a, b.

The data given confirm that thermocapillary convection has a clearly expressed near-surface character. It makes a substantial contribution to the heat flux on the disk edge but virtually does not influence the axial region under the disk, and in the integral heat flux for comparable values of Gr and Ma its contribution is not substantial. The amplitude of the velocity along the free surface in thermocapillary convection is higher than in the regime of thermogravitational convection. The local maxima of $U(r, H)$ coordinated with radial temperature gradients along the surface. Against the background of thermogravitational convection the influence of the thermocapillary effect manifests itself in the increase of the speed directly on the free surface, but the amplitude of the speed decreases in comparison with the regime of thermocapillary convection because of the equalization of temperature along the free surface owing to gravitational convection and the effect of temperature stratification of the liquid in the gravity field.

This work was carried out with financial support from the Russian Foundation for Basic Research (project code 99-01-00544) and Integration Projects of the Siberian Branch of the Russian Academy of Sciences, Nos. 2000-49 and 2000-55.

## NOTATION

$t$, time; $r$ and $z$, variables in the cylindrical coordinate system; $H$, height of the layer of liquid in the crucible; $U$, radial component of the velocity vector; $V$, axial component of the velocity vector; $T$, tempera-

ture; $\psi$, stream function; $\theta$, dimensionless temperature; $\omega$, vortex; $\Delta$, Laplace operator in the cylindrical coordinate system; $\mu$, coefficient of dynamic viscosity; $\nu$, coefficient of kinematic viscosity; $\alpha$, thermal diffusivity; $g$, gravity acceleration; $\beta$, thermal-expansion coefficient; $\sigma$, surface-tension coefficient; $R_\alpha$, radius of the crystal; $R_{cr}$, radius of the crucible; $q$, heat flux; $\mathrm{Gr} = \frac{g\beta}{\nu^2}\Delta T R_d^3$, Grashof number; $\mathrm{Ma} = \left(-\frac{\partial\sigma}{\partial T}\right)\frac{R_d}{\alpha\mu}\Delta T$, Marangoni number; $\mathrm{Pr} = \frac{\nu}{\alpha}$, Prandtl number; Nu, Nusselt number; $\mathrm{Re} = \frac{\omega R_d}{\nu}$, Reynolds number; $\Delta T \equiv T_{cr} - T_d$, temperature difference. Subscripts: d, crystal (disk); cr, crucible.

## REFERENCES


1. V. S. Berdnikov, V. L. Borisov, V. A. Markov, and V. I. Panchenko, in: *Hydromechanics and Heat and Mass Transfer in Production of Materials* [in Russian], Moscow (1990), pp. 68–88.
2. V. S. Berdnikov, V. I. Panchenko, and S. V. Solov'ev, in: *Proc. III Minsk Int. Forum "Heat and Mass Transfer – MIF-96"* [in Russian], Vol. 11, May 20–24, 1996, Minsk (1996), pp. 146–150.
3. V. S. Berdnikov, V. I. Polezhaev, and A. I. Prostomolotov, *Izv. Akad. Nauk SSSR, Mekh. Zhidk. Gaza*, No. 5, 33–40 (1985).
4. V. S. Berdnikov, V. V. Vinokurov, V. I. Panchenko, and S. V. Solov'ev, in: *Proc. 4th Int. Conf. "Actual Problems of Electronic Instrument Making"* [in Russian], Vol. 3, Novosibirsk (1998), pp. 53–61.
5. V. S. Berdnikov, V. I. Panchenko, and S. V. Solov'ev, in: *Thermal Physics of Crystallization and High-Temperature of Material Treatment* [in Russian], Novosibirsk (1990), pp. 162–199.
6. V. I. Polezhaev, A. V. Buné, N. A. Verezub, et al., *Mathematical Modeling of Convective Heat Transfer on the Basis of the Navier–Stokes Equations* [in Russian], Moscow (1987).
7. A. A. Samarskii, *Introduction to the Theory of Difference Schemes* [in Russian], Moscow (1971).